Practical Application of CFRP Strengthening to Steel Floor Beams with Web Openings: A numerical investigation

Mohammed Altaee[a], Lee S. Cunningham[b], Martin Gillie[c]

[a] University of Babylon, College of Engineering, Hilla, Iraq

[b] University of Manchester, School of Mechanical, Aerospace & Civil Engineering, Manchester, UK

[c] University of Warwick, School of Engineering, Coventry, UK

ABSTRACT: Strengthening of existing steelwork is often necessary where a change of use or geometric modifications are made. In the case of floor beams, it is particularly common to introduce web openings to accommodate services such as air conditioning etc. The use of carbon fibre reinforced polymer composites (CFRP) overcomes several of the difficulties associated with the use of traditional strengthening techniques with welded steel plate. CFRP has a superior strength to weight ratio than steel and has excellent corrosion resistance. In comparison to welded plate, CFRP is generally easier to handle and apply. Currently there is a scarcity of research on the application of CFRP to steel beams with web openings and the work that does exist is limited to relatively small-scale beams. In the present work a numerical model validated against experimental work by the authors is used investigate the application of CFRP to floor beams common in everyday practice. The results show that practical and efficient layouts of CFRP can be used to achieve similar or greater strengthening effect in comparison to traditional steel plate methods.

Keywords: CFRP, strengthening, steel floor beams, web openings

1. Introduction

During the life of an existing steel frame building, there is often a need to introduce openings into the webs of floor beams. This may be driven by change of use or simply enhanced service requirements such as air-conditioning, information technology services etc. Often such openings constitute a substantial local reduction in web steel and hence require strengthening to allow the floor beam to maintain its design load capacity. Traditionally strengthening is provided in the form of welded steel plate stiffeners, however this technique can have inherent practical difficulties. The use of fibre reinforced polymer composite plates adhesively bonded to the steel surface has the potential to offer a highly practical solution in this case. Carbon fibre reinforced polymers (CFRP) are increasingly being used as an alternative to welded steel plates to strengthen steel structures due to their outstanding mechanical properties ($E \approx 1{,}200$MPa and $\sigma_{ult} \approx 140$GPa). In addition, CFRP laminates are typically less than 1/5 the density of steel and are corrosion resistant [1]. This paper explores the use of CFRP in

strengthening web openings in floor beams of the kind of span and loading consistent with modern commercial frame buildings.

2. Existing work on CFRP strengthening of steel sections

To date, many experimental works and theoretical studies have been conducted on the bonding of CFRP to steel beams, each focussing on a different parameter. Most commonly in the case of I-sections, CFRP is applied to the tension flange for flexural strengthening. Edberg *et al.* [2] presented experimental research in which five various configurations of Carbon Fibre Reinforced Polymer (CFRP) and Glass Fibre Reinforced Polymer (GFRP) plates were bonded to the tensile flange of W8x10 steel beams of 1372mm span. The first scheme consisted of 1219mm long, 4.6mm thick CFRP plate bonded directly to the tension flange. In the second scheme, a honeycombed aluminium plate was placed between the tension flange and CFRP to increase the moment of inertia of the section. In the third scheme a foam core was attached to the tension flange, followed by wrapping the whole assembly in a GFRP sheet. The fourth scheme consisted of a pultruded GFRP channel bonded both adhesively and mechanically to the tension flange. All specimens were tested under four-point bending tests. The recorded increase in ultimate load compared to the un-strengthened beam ranged from 37% to 71%, with the second strengthening scheme exhibiting the greatest enhancement, a similar trend was observed in the recorded enhancement in stiffness.

Deng & Lee [3] used different lengths and thicknesses of CFRP (E = 212GPa) in strengthening ten 127×76×13UKB steel I-sections of 1100mm span under either three or four points static bending. The dominant mode of failure of the strengthening system observed in the experimental series was that of de-bonding of the CFRP plate. It was concluded that de-bonding was initiated at lower load levels when the CFRP plate thickness increased and its length decreased. The maximum gain in strength (30%) was achieved in the beam with the longest bonded length, 500mm, and thinnest CFRP plate thickness, 3mm.

Gillespie *et al.* [4] conducted cyclic loading tests on a series of naturally corroded bridge girders, 9754mm in length, 610mm deep. The test included using a single layer of CFRP, 6.4mm thick and 38.1 mm in width, to reinforce the entire length of the bottom flanges of two girders, these areas being more affected by corrosion than the webs or top flanges. The results of this study showed that CFRP reinforcement increased the elastic stiffness and the ultimate capacities of the girders by 17% and 25%. Tavakkolizadeh & Saadatmanesh, [5] used four-point bending on two groups of S5x10 steel beams, 1300mm long, which were notched in the middle of the tension flange to different depths of 3.2mm and 6.4mm. Both groups were strengthened by different lengths of 0.13mm thick CFRP sheets. The results showed that the ultimate load carrying capacity and stiffness of retrofitted specimens were close to their original values in the control specimens without notches regardless of the length of the CFRP patch.

Some researchers have focused on the strengthening system's bond with the steel substrate and the ability to maintain stress transfer between the steel and CFRP. This transfer is affected by many factors such as surface preparation, bonded length, type of adhesive material, thickness of adhesive and thickness of CFRP laminate. To provide sufficient roughness and adequate bond strength, the steel surface needs to be prepared appropriately. An experimental study by Bocciarelli *et al.* [6] on fatigue failure showed that de-bonding of CFRP plates starts in the zones of high stress concentration at the plate ends. Youssef [7] also concluded that the maximum value of the adhesive shear stress occurs at the edges of the FRP sheet. Zhoa and Zhang [8] studied the possible failure modes associated with the bonding of CFRP to steel subjected to a tensile force. The work by [9] showed that bonding failure or delamination between steel and CFRP is considered the most common failure of the strengthening system due to the weakness of the adhesive bond. Given the relative weakness of the bond interface, a number of researchers have investigated use of unbonded pre-stressed CFRP plate as means of retrofitting steel structures e.g. Kianmofrad et al [10] and the technique has recently been used in the field to strengthen full scale bridge girders of historic steel construction, Ghafoori et al [11], Hosseini et al. [12].

All the aforementioned studies concentrated on steelwork without openings. To date, there is a scarcity of research focussing on the specific application of strengthening web openings. One of the first available numerical studies in this area is that conducted by Mahmoud [13] in which small scale beams (150mm deep I-sections) with 30mm x 30mm web openings were simulated using the FE package ANSYS, de-bonding was not modelled. Two separate CFRP plate positions were examined; CFRP on the bottom flange and CFRP plate across the entire web around the opening. A notable enhancement in strength was gained in both cases. Recently, for the specific case of deep plate girders with discrete web openings, shear buckling behaviour has been studied by Hamood *et al.* [14]. The girders were 600mm deep and had a clear span of 1200mm, four were strengthened with 1.13mm thick CFRP strips positioned on the web around the opening. Two web opening shapes were examined, square and diamond, with 40 percent of the web depth as an edge length of the opening. The results show that an increase in the ultimate shear load was achieved, ranging from 8.7% to 21.5% for the CFRP-strengthened girders compared to the corresponding un-strengthened cases.

The present authors conducted the first full-scale experimental and numerical work in this application and demonstrated the general feasibility of the CFRP technique in the case of large rectangular web openings, Altaee *et al*. [15,16,17]. However, the beams examined in the previous studies had limited depth and spans, i.e. 3m. For practical application of the CFRP strengthening technique to floor beams, it is important to demonstrate its capability when applied to spans and loads commensurate with modern commercial frame buildings. In parallel with capability, it is equally important to show that efficient configurations of CFRP strengthening can be used to gain similar strengthening effect to that of traditional steel plate strengthening. In the present paper, a validated finite element model using the software ABAQUS 6.13-1 is used to explore the aforementioned full-scale application of the CFRP strengthening technique.

3. Finite element model validation

This section validates the finite element modelling approach used in this study against an experimental series previously undertaken by the authors, Altaee *et al.* [15, 16]. The series consisted of 4 no. 305×102×25 UKBs with 3m clear span; one without a web opening acting as the control (B0), and three with rectangular web openings in different locations (B1, B2 and B3). CFRP reinforcement was applied at the web openings both on the web and flanges as shown in Figure 1.

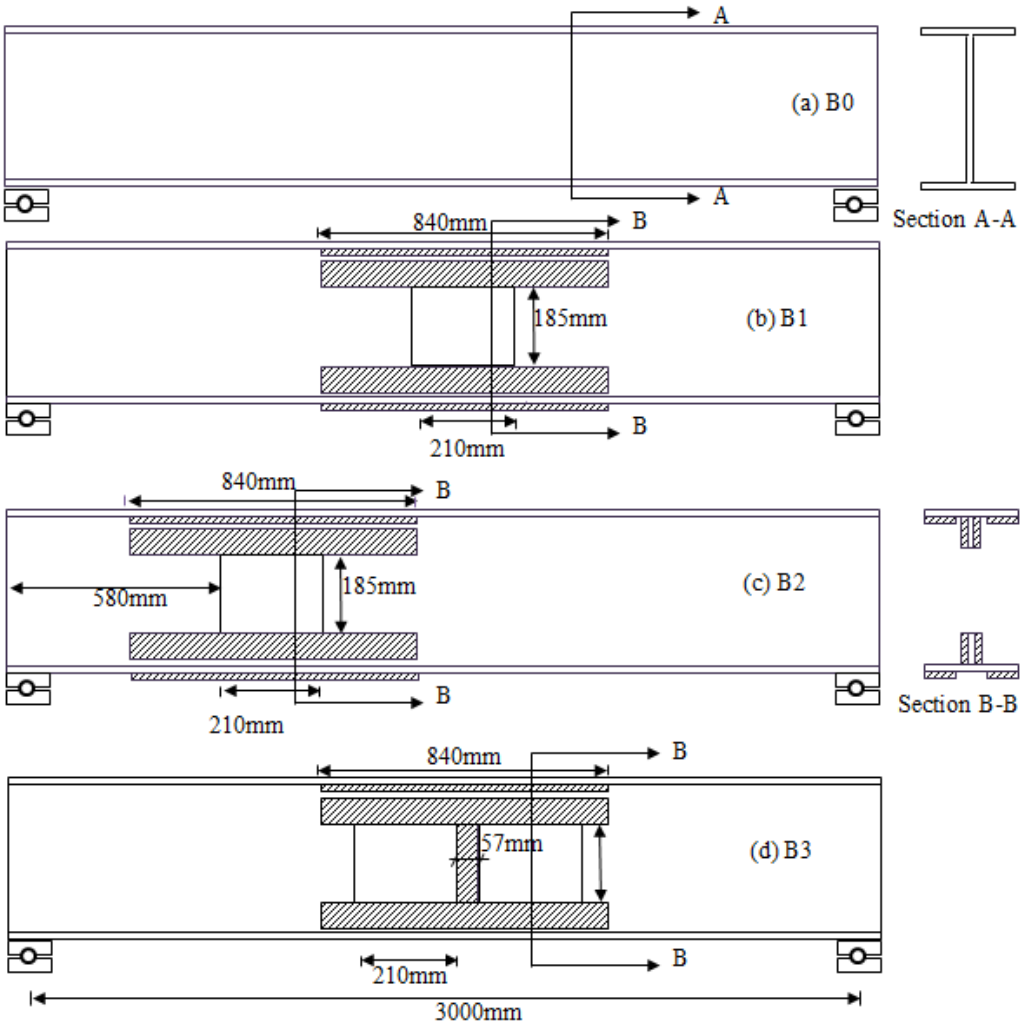

Figure 1: Schematic of strengthening layouts used in Altaee *et al*'s previous experimental study [17].

3.1 Loading and Boundary Conditions

Numerical models of each test were created with the same the loading and boundary conditions as in the experiments (Figure 2). In the experiments, steel bearing plates (300mm×130mm×30mm) were placed at the supports and under the point loads. To model these, a "hard interaction" condition was implemented numerically to simulate contact between the plates and the specimen. A lubricant was applied to the bottom flange support plates in the tests so a friction coefficient of 0.16 was specified

numerically at these locations. By contrast no lubricant was applied at the loading points so a friction coefficient of 0.8 [18] was specified here. Additionally, the top flange of the beam in the model was laterally restrained at 4 discrete points, representing the lateral restraints present in the tests.

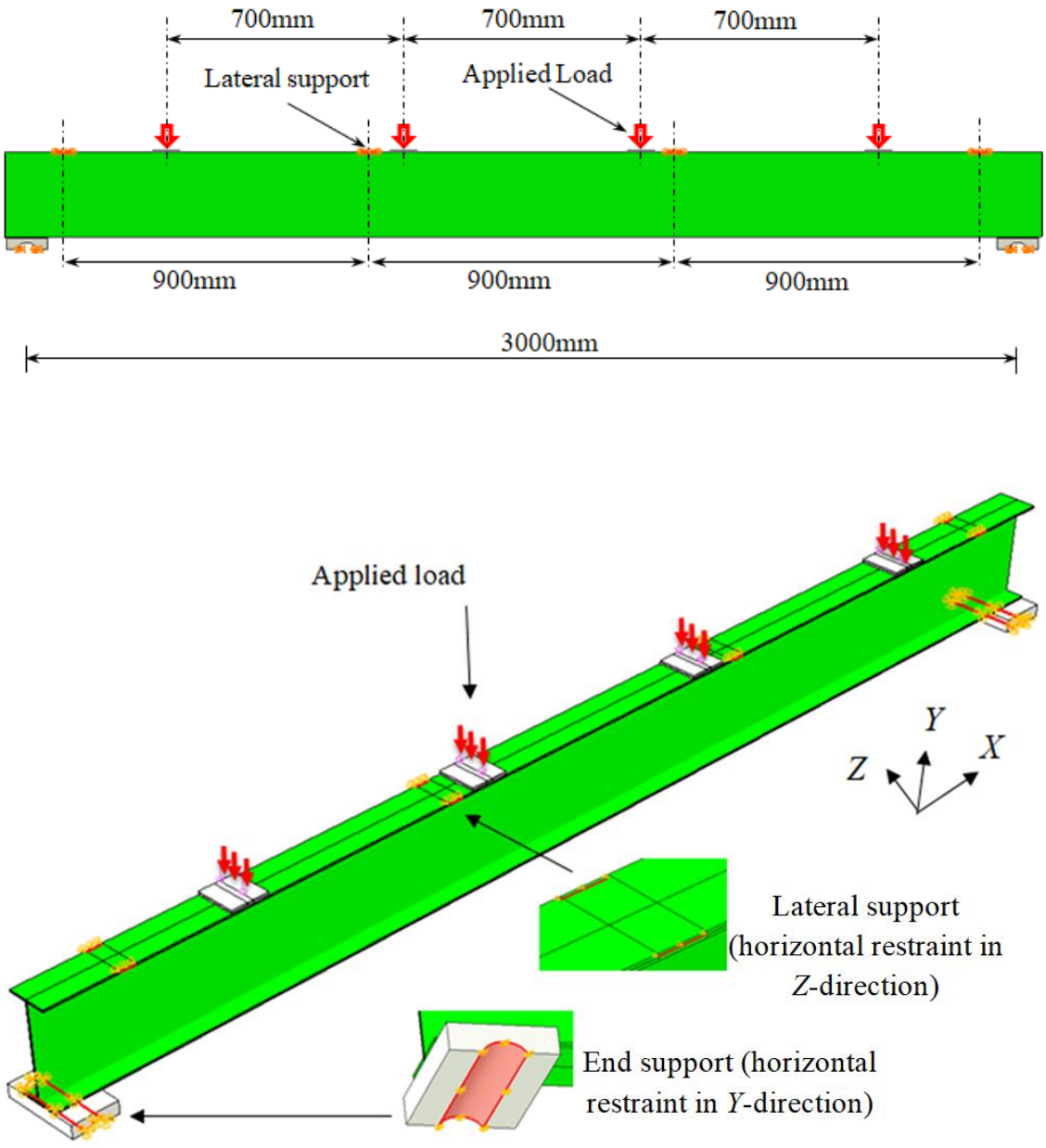

Figure 2: Test specimen load & boundary conditions.

3.2 Material models

All materials properties were extracted from [17] and shown in Tables 1-3. Steel was modelled as a plastic isotropic material using the four-noded shell element S4R. The CFRP was also modelled with this element but with linear elastic behaviour. Element type COH3D8, an eight-node, three-dimensional cohesive element including traction-

separation behaviour was used to model the adhesive material between the steel and CFRP.

To capture any potential de-bonding of the CFRP plate from the steel substrate a bilinear traction-separation law was used, see Figure 3, where the softening after damage initiation is linear. The same approach in has been validated by Al-Mosawe et al. [19] who used Abaqus to successfully simulate the bond behaviour of CFRP laminate and steel members subject to static and dynamic loads. The same type of adhesive used in the current work was studied i.e. Araldite 420 epoxy [20]. In the work by Al Mousawe et al. [19], a total of 228 CFRP strengthened steel joints in shear were tested experimentally to provide a basis for the model validation. The same model has also recently been implemented by Kadhim et al. [21] to obtain accurate simulations of the bond behaviour of CFRP strengthened steel hollow section beams and columns under both static and dynamic loads.

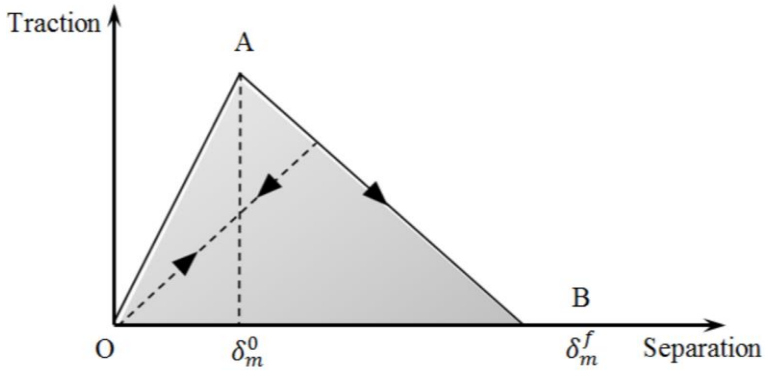

Figure 3: Illustration of a simple bilinear traction-separation law, based on [22].

The implemented damage model consists of two stages, a damage initiation and a damage evolution. The quadratic nominal stress criterion is used as the damage initiation criterion [22], which can be represented as:

$$\left(\frac{\langle t_n \rangle}{\sigma_{\max}}\right)^2 + \left(\frac{t_s}{\tau_{\max}}\right)^2 + \left(\frac{t_t}{\tau_{\max}}\right)^2 = 1 \qquad 1$$

where, t_n, t_s and t_t are peak values of the nominal stress.

σ_{max} is the tensile strength of the adhesive, and

τ_{max} is the shear strength of the adhesive; the symbol < > represents the Macaulay bracket which is used to signify that compressive stresses do not initiate damage (i.e. t_n is negative and thus $<t_n>$ is equal to zero). Note that for the adhesive used in this study σ_{max} and τ_{max} are given in table 2, these are based on the manufacturers' declared test values.

After damage initiation, a scalar damage variable D is introduced as the overall damage in the material. The range of D is from 0 to 1, with 0 representing the undamaged case

and 1, the total separation. Following this the corresponding stress components are then degraded as follows [22]:

$$t_n = \begin{cases} (1-D)\ \bar{t}_n & ,\bar{t}_n \geq 0 \\ \bar{t}_n & ,\bar{t}_n \langle 0 \end{cases} \quad 2$$

$$t_t = (1-D)\ \bar{t}_t$$
$$t_s = (1-D)\ \bar{t}_s \quad 3$$

where, $\bar{t_n}, \bar{t_t}$ and $\bar{t_s}$ are the stress components predicted by multiplying the initial stiffness and the current relative displacements. For a linear softening law, the damage index *D* can be expressed as [22]:

$$D = \frac{\delta_m^f (\delta_m^{\max} - \delta_m^0)}{\delta_m^{\max} (\delta_m^f - \delta_m^0)} \quad 4$$

where $\delta_m^{\max}$ is the maximum effective relative displacement attained during the loading history, and δ_m^0 and δ_m^f are the effective relative displacement at the initiation and end of failure respectively. The effective relative displacement δ_m^f can be written as [22]:

$$\delta_m^f = \sqrt{\langle \delta_n \rangle^2 + \delta_s^2 + \delta_t^2} \quad 5$$

To achieve an efficient mesh, four mesh schemes were examined by varying the number of elements along the width of the flange, web and along the beam length for the control beam (B0-FE), as shown in Table 4 and Figure 4. The results for the mid-span deflection versus the load for the selected meshes show a good convergence with the corresponding experimental results in terms of stiffness and ultimate load, except for mesh 4 which was unable to match the experimental ultimate load and produced a less stiff post-peak response compared to the other mesh arrangements. Given the lack of difference between meshes 1, 2 and 3, mesh 3 was adopted for efficiency (Figure 5).

Table 1: Summary of the mechanical properties of steel [17].

	Young's Modulus (GPa)	Yield stress (MPa)	Ultimate tensile stress (MPa)
Flange	206	412	566
Web	210	435	569

Table 2: Summary of the mechanical properties of adhesive [20].

Young's Modulus (GPa)	Ultimate Tensile strength (MPa)	Ultimate Shear strength (MPa)	Strain at rupture %
1.5	29	26	4.6

Table 3: Summary of the mechanical properties of CFRP plates [17].

Young's Modulus (GPa)	Ultimate Tensile strength (MPa)	Thickness (mm)	fibre volumetric content %
200	2970	3	70

Table 4: Number of divisions for the mesh schemes of beam B0-FE.

Mesh scheme	Number of elements along the web height	Number of elements across the flange width	Number of elements along the beam length
1	30	10	300
2	20	6	200
3	12	4	120
4	9	2	85

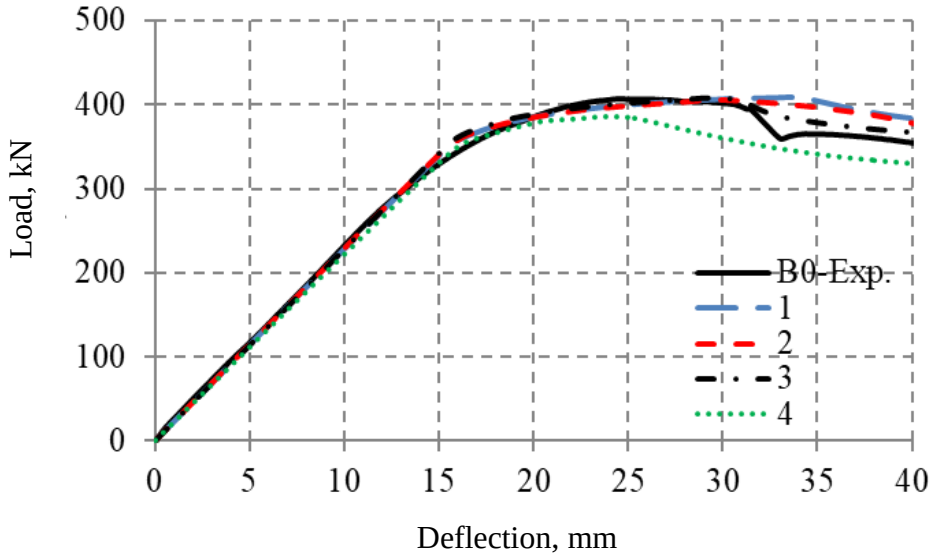

Figure 4: Load vs. mid-span deflection behaviour for different mesh arrangements.

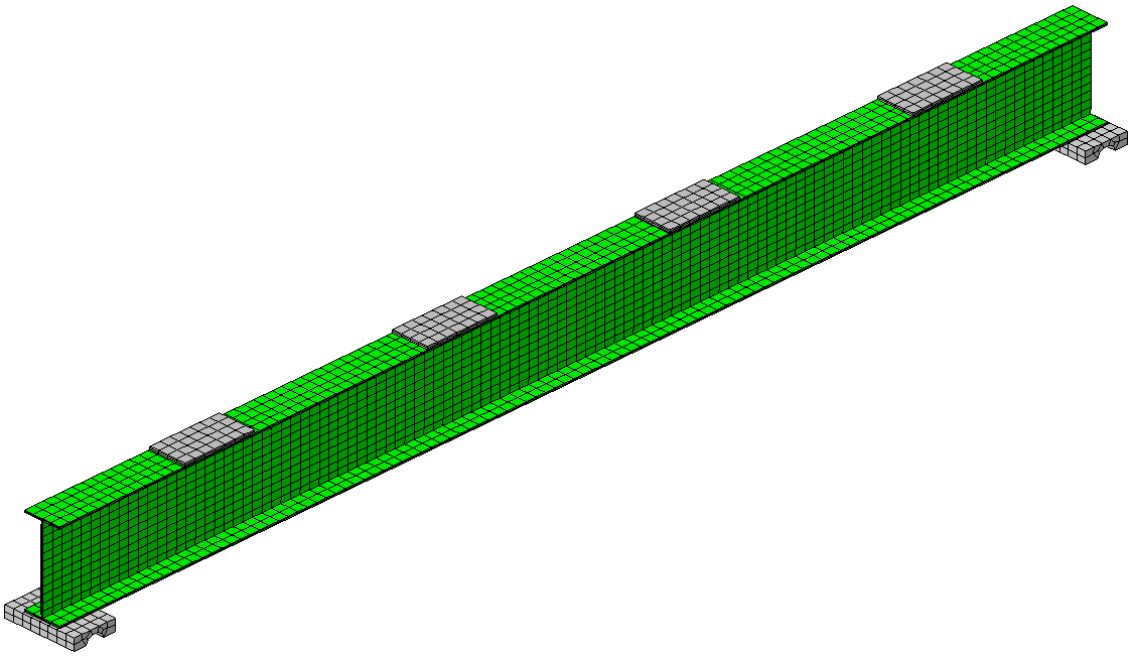

Figure 5: Diagram of final chosen mesh (mesh scheme no.3).

3.3 Simulation results

3.3.1 Load-deflection behaviour

The load-deflection curves measured at the beam's mid-span in the experiments and those from the numerical simulation are presented in Figure 6 for all beams. For all simulations, the numerical model gives reasonable agreement with the experimental results of Altaee *et. al.* [17]. The numerical models show very similar stiffness to the experimental beams while the slight over-predicting the maximum loads (by 1%, 2%, 4% and 5% for B0, B1, B2 and B3 respectively.) In the lead up to maximum loads, all models have a deviation of less than 2% in terms of the load-displacement behaviour.

The failure modes were also similar to those occurring in the experiment as shown in Figures 7-10. The yielding of the top flange was followed by torsional buckling at mid-span of beams B0 and B2, while in B1 and B3 debonding at the ends of the CFRP occurred at the top flange.

There was good agreement between readings from strain gauges mounted on the CFRP and steel in beams B1, B2 and B3 and the numerical results, as shown in Figure 11. All numerical strain values without exception follow the same trend as the corresponding experimental values. The majority of the numerical strain versus load values are within 10% of the corresponding experimental values. These results show that the model is capable of capturing the behaviour of CFRP strengthened steel beams to with a good level of accuracy.

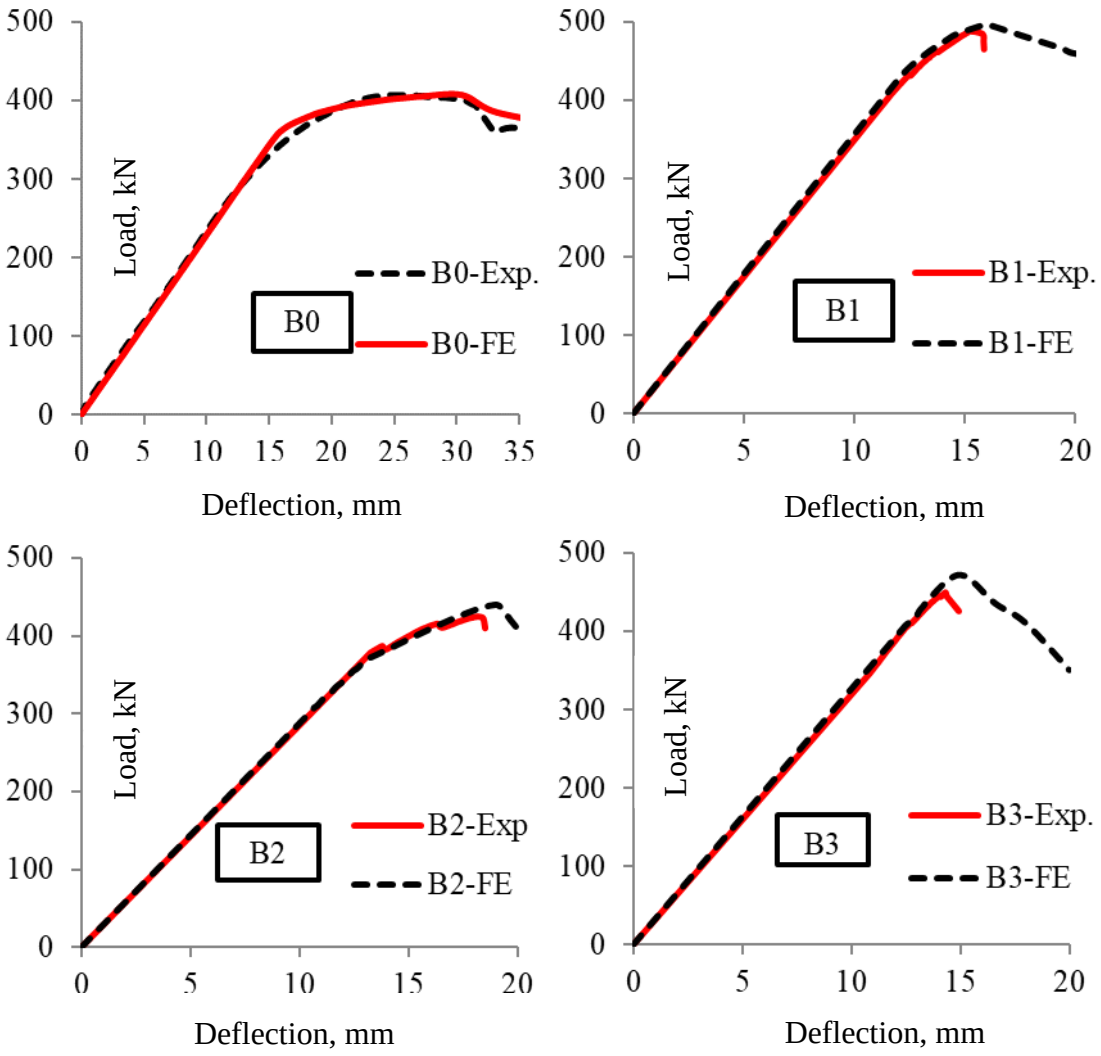

Figure 6: Load vs. mid-span deflection of beam B1, B2 and B3.

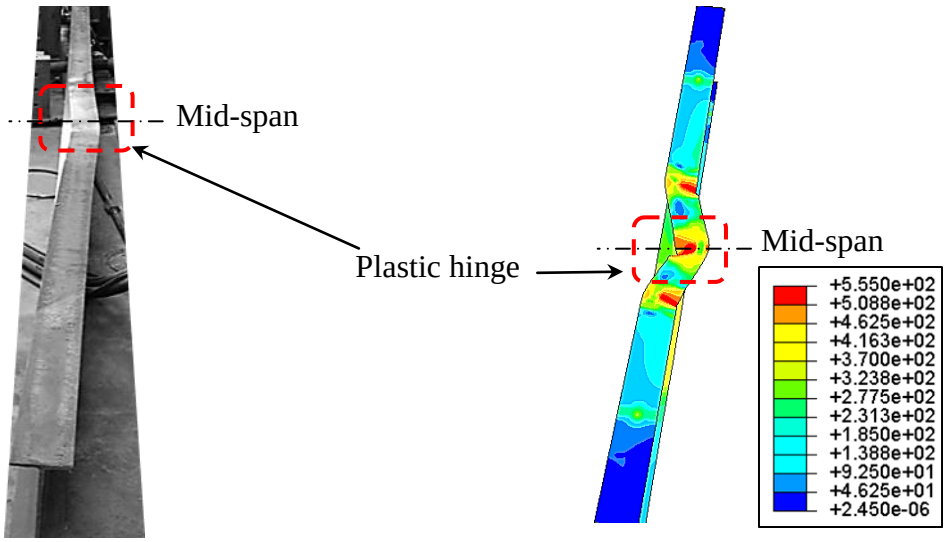

Experimental failure mode

Von Mises stress distribution, MPa, in FE model

Figure 7: Failure patterns for specimens B0-FE and B0-Exp. at maximum load.

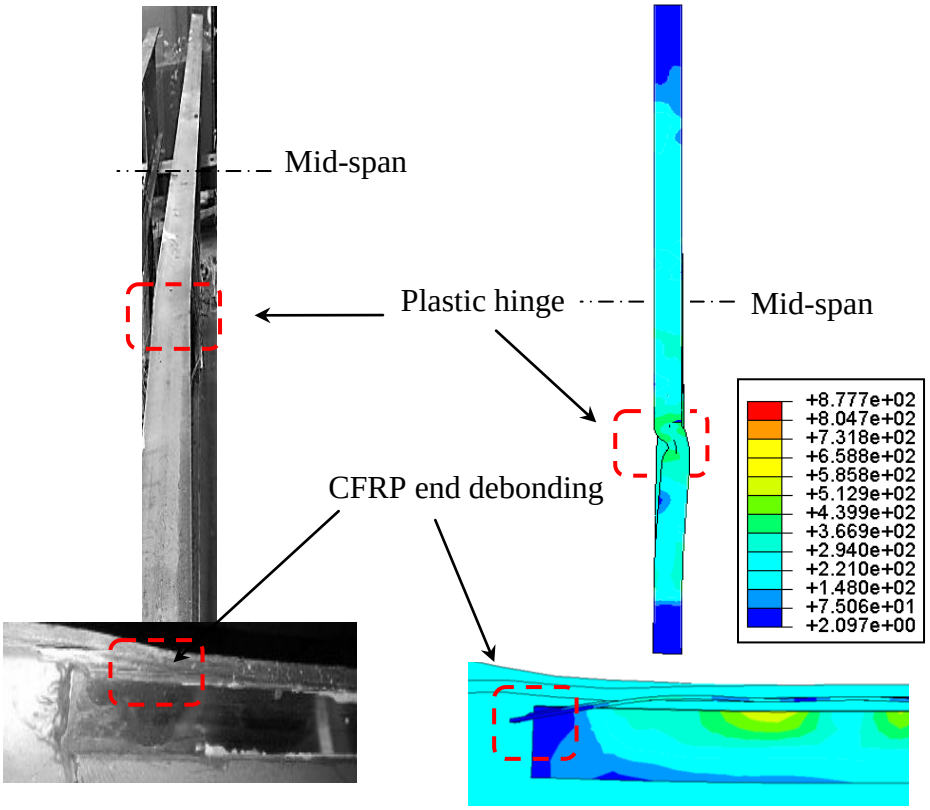

Figure 8: Failure patterns for specimens B1-FE and B1-Exp.at maximum load.

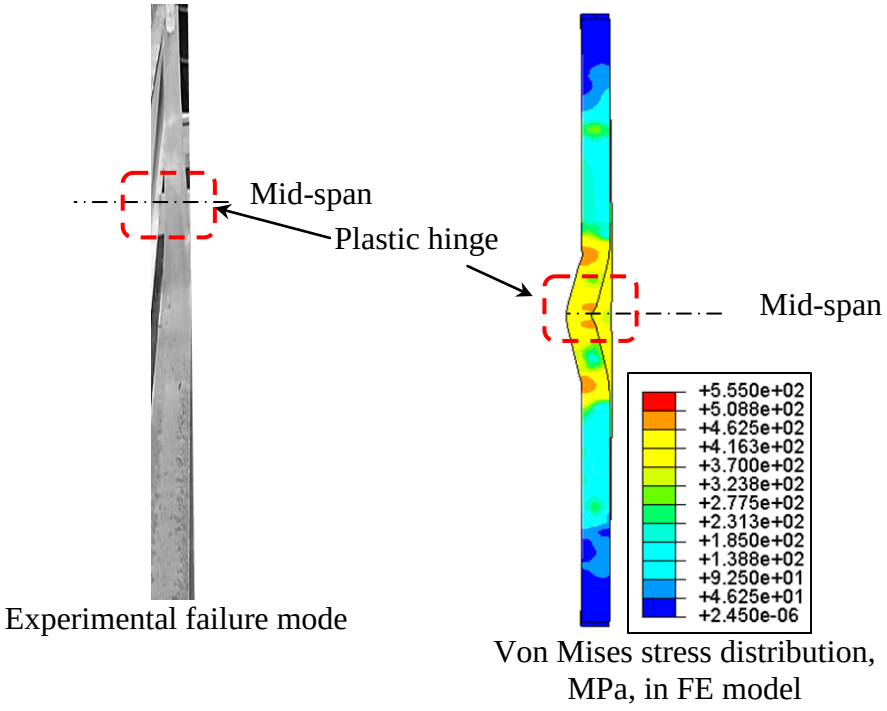

Figure 9: Failure patterns for specimens B2-FE and B2-Exp. at maximum load.

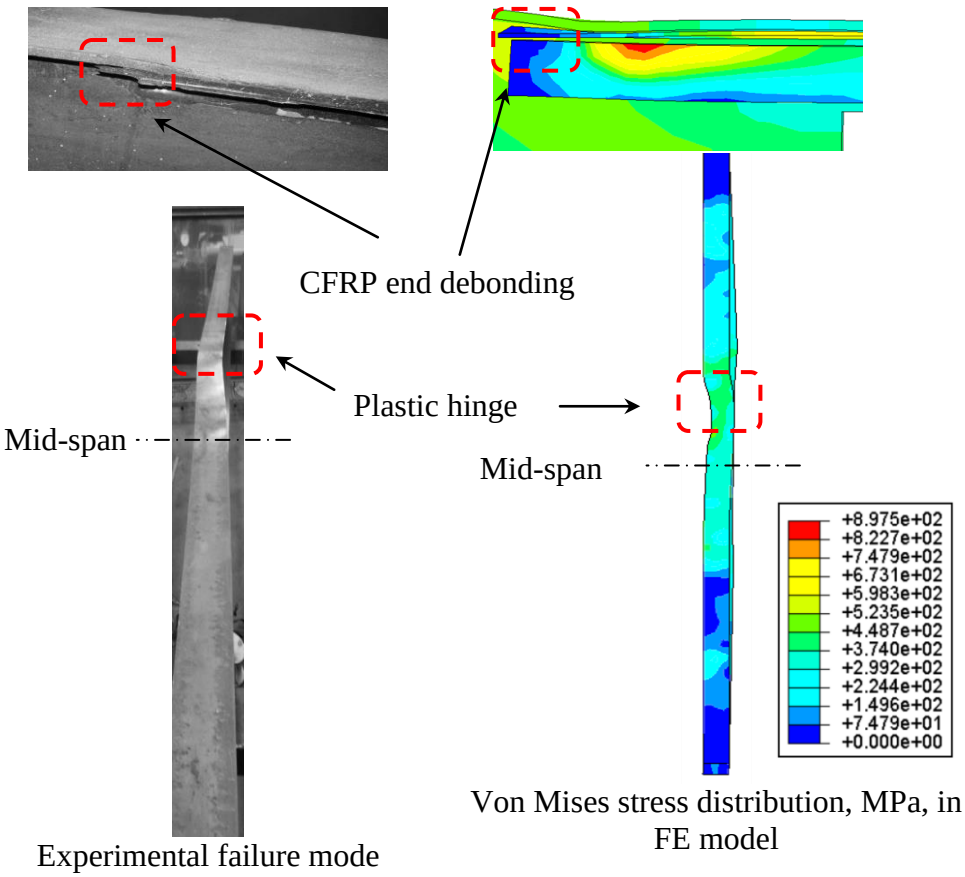

Figure 10: Failure patterns for specimens B3-FE and B3-Exp. at maximum load.

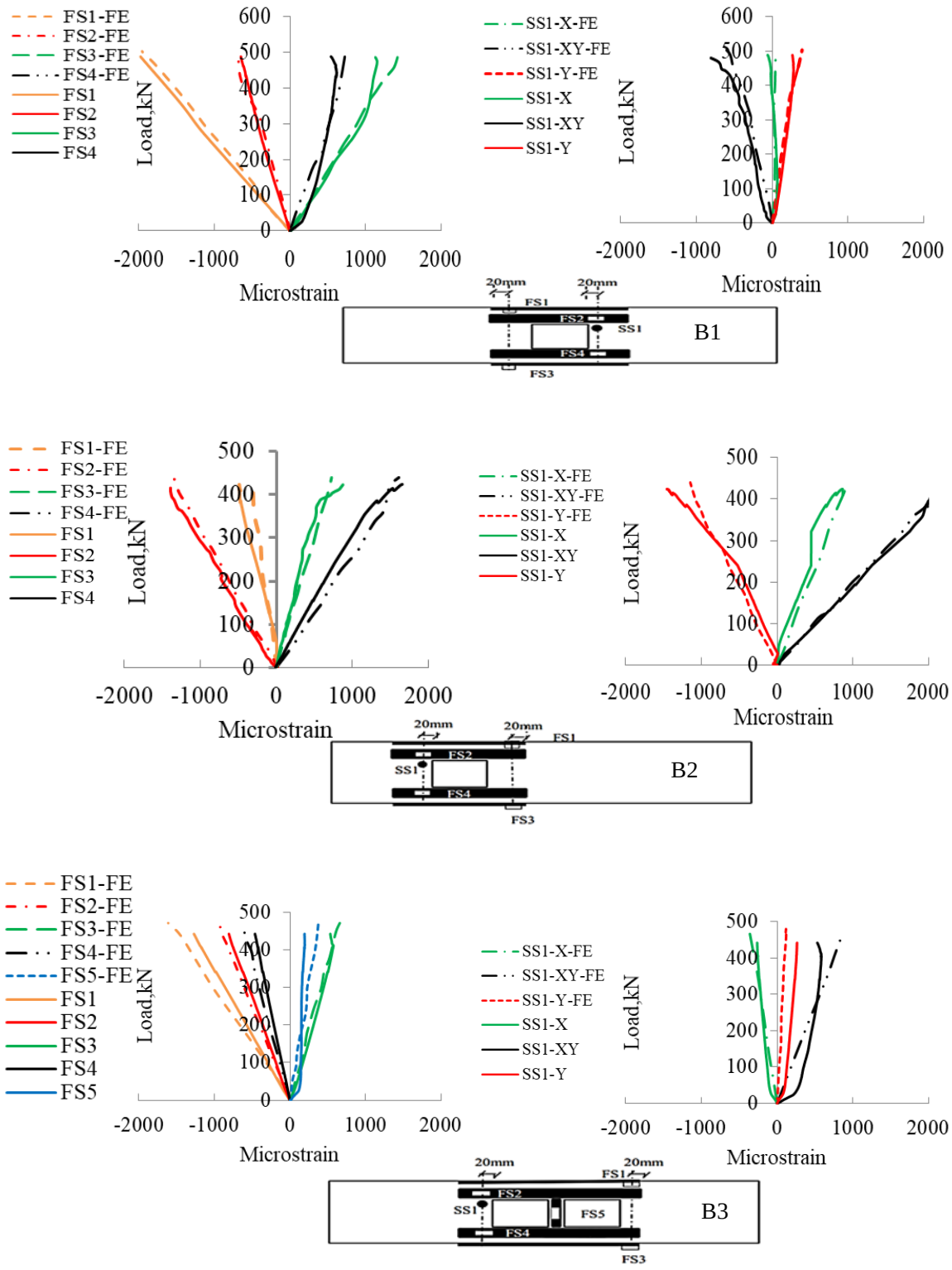

Figure 11: Comparison of experimental and numerical strains in steel and CFRP for beams in B1, B2 and B3.

4. Case Study

The purpose of this section is to explore the application of the CFRP strengthening technique to larger beams than those studied experimentally [17] in typical structural grids and to investigate whether there are practical size limits to the applicability for CFRP strengthening. Additionally, the performance of CFRP strengthening will be compared with conventional steel-plate strengthening. In total 42 beams will be examined, with variation in beam span and opening size and location. As beam spans increase, the opening size is increased and correspondingly the area and thickness of CFRP strengthening increases. The same general configuration of CFRP strengthening is used throughout.

4.1 Model description and material properties

To represent typical commercial floor arrangements, three different bay sizes (representing column centre to centre positions in each direction) of 7.5×7.5m, 10×10m and 15×15m were framed using primary and secondary beams (Figure 12). In each case three secondary beams were assumed in each bay. The steel beams were sized in accordance with Eurocode 3 [23], (Table 5). All beams were designed as simply supported with unfactored live dead loads of 5kN/m^2 and 3.6kN/m^2 (representing a 150mm thick reinforced concrete slab) respectively according to Eurocode 1[24]. The top flanges of the beams were assumed to be fully laterally restrained.

Following initial design, each beam (primary and secondary) had a web opening introduced. The opening length was taken 0.75 of the beam depth and the opening height as 0.6 of the beam depth, whether located at mid-span or near the supports, as shown in Figure 13 and described in Table 6. The configuration of CFRP strengthening originally suggested by Altaee *et. al* [17] is used here, with CFRP strips having a length of four times the opening length (Figure 13). The material properties of the CFRP and adhesive material used here were the same as those extracted from the experimental test and presented in Section 2. The steel was assumed to be of grade S355 and the stress-strain curve is shown in Figure 14. The steel density and the modulus of elasticity were 7850 kg/m^3 and 200 GPa respectively. The steel-plate strengthening has been designed in accordance with the SCI P355 [25] guidance with the same steel properties for the steel beam. The stiffeners were welded on both sides of the steel web, above and below the openings, see Figure 12, with the same steel properties for the steel beam.

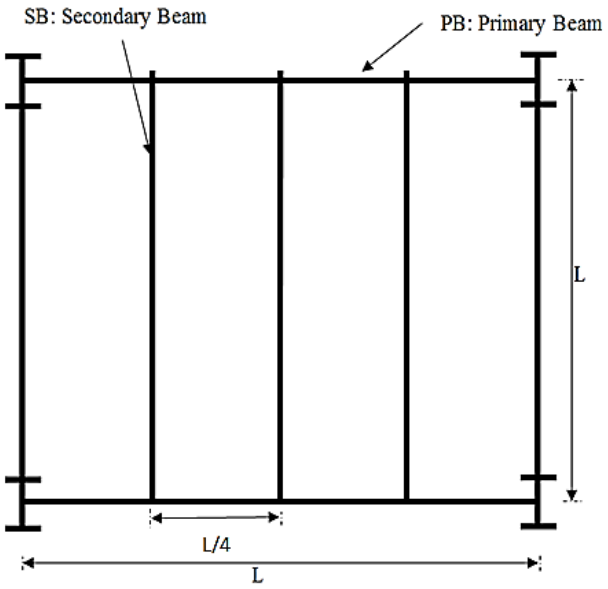

Figure 12: Schematic of floor beam layout.

Table 5: Beam sections (based on UK Universal Beam Designations).

	7.5m	10m	15m
PB	533×312×273	914×419×343	1500×310×1020
SB	305×127×48	457×152×74	686×254×125

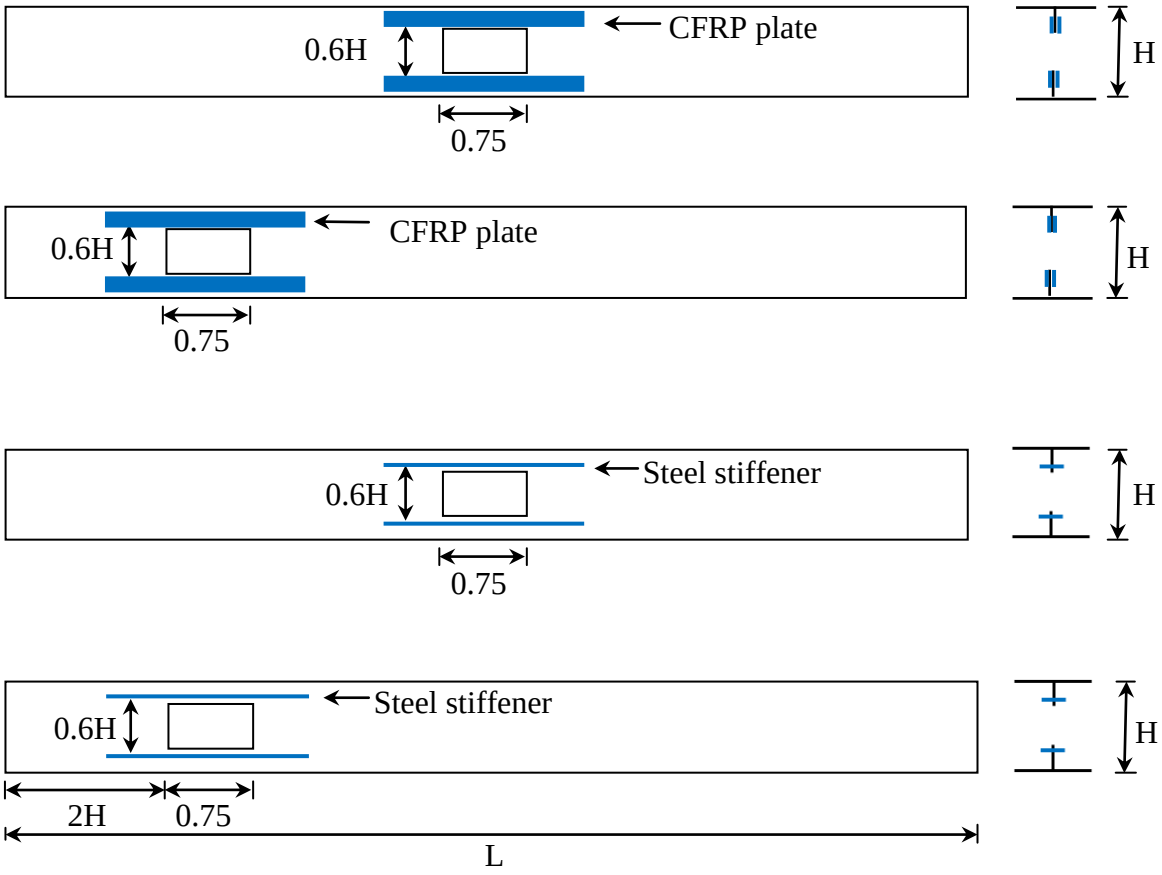

Figure 13: Schematic of strengthening arrangements.

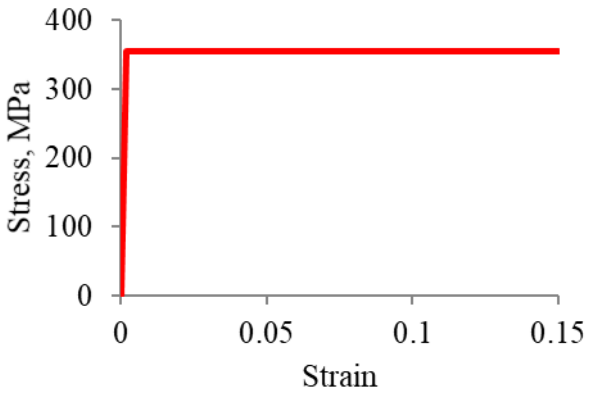

Figure 14: Steel stress-strain relationship used in the current simulations.

Table 6: Description of beams used in the all floors.

Beam nomination	Beam section	Opening size, mm	Steel plate/CFRP strengthening			Description
			thickness, mm	length, mm	width, mm	
PB0-7.5	533×312×273	-	-	-	-	Reference primary beam without opening or strengthening with 7.5m span.
PB1-UO-7.5		404.6×323.7	-	-	-	Primary beam with unreinforced opening at mid-span with 7.5m span.
PB2-UO-7.5			-	-	-	Primary beam with unreinforced opening at shear region with 7.5m span.
PB1-ROS-7.5			12	800	80	Primary beam with steel plate reinforced opening at mid-span with 7.5m span.
PB1-ROC-7.5			5.4	1618	125	Primary beam with CFRP reinforced opening at mid-span with 7.5m span.
PB2-ROS-7.5			12	800	80	Primary beam with steel plate reinforced opening at shear region with 7.5m span.
PB2-ROC-7.5			3	1618	125	Primary beam with CFRP reinforced opening at shear region with 7.5m span.
SB0-7.5	305×127×48	-	-	-	-	Reference secondary beam without opening or strengthening with 7.5m span.
SB1-UO-7.5		233×186.6	-	-	-	Secondary beam with unreinforced opening at mid-span with 7.5m span.
SB2-UO-7.5			-	-	-	Secondary beam with unreinforced opening at shear region with 7.5m span.
SB1-ROS-7.5			5	470	80	Secondary beam with steel plate reinforced opening at mid-span with 7.5m span.
SB1-ROC-7.5			2	933	50	Secondary beam with CFRP reinforced opening at mid-span with 7.5m span.
SB2-ROS-7.5			5	470	80	Secondary beam with steel plate reinforced opening at shear region with 7.5m span.
SB2-ROC-7.5			1.3	933	50	Secondary beam with CFRP reinforced opening at shear region with 7.5m span.
PB0-10	914×419×343	-	-	-	-	Reference primary beam without opening or strengthening with 10m span.
PB1-UO-10		683.8×547	-	-	-	Primary beam with unreinforced opening at mid-span with 10m span.
PB2-UO-10			-	-	-	Primary beam with unreinforced opening at shear region with 10m span.
PB1-ROS-10			10	1350	150	Primary beam with steel plate reinforced opening at mid-span with 10m span.
PB1-ROC-10			4.6	1618	165	Primary beam with CFRP reinforced opening at mid-span with 10m span.
PB2-ROS-10			10	1350	80	Primary beam with steel plate reinforced opening at shear region with 10m span.

PB2-ROC-10			2.8	1618	165	Primary beam with CFRP reinforced opening at shear region with 10m span.
SB0-10	457×152×74	-	-	-	-	Reference secondary beam without opening or strengthening with 10m span.
SB1-UO-10		346.5×277.2	-	-	-	Secondary beam with unreinforced opening at mid-span with 10m span.
SB2-UO-10			-	-	-	Secondary beam with unreinforced opening at shear region with 10m span.
SB1-ROS-10			5	700	100	Secondary beam with steel plate reinforced opening at mid-span with 10m span.
SB1-ROC-10			2.4	1386	60	Secondary beam with CFRP reinforced opening at mid-span with 10m span.
SB2-ROS-10			5	700	100	Secondary beam with steel plate reinforced opening at shear region with 10m span.
SB2-ROC-10			1.4	1386	60	Secondary beam with CFRP reinforced opening at shear region with 10m span.
PB0-15	1500×310×1020	-	-	-	-	Reference primary beam without opening or strengthening with 15m span.
PB1-UO-15		1125×900	-	-	-	Primary beam with unreinforced opening at mid-span with 15m span.
PB2-UO-15			-	-	-	Primary beam with unreinforced opening at shear region with 15m span.
PB1-ROS-15			20	2200	80	Primary beam with steel plate reinforced opening at mid-span with 15m span.
PB1-ROC-15			11.4	1618	135	Primary beam with CFRP reinforced opening at mid-span with 15m span.
PB2-ROS-15			20	2200	80	Primary beam with steel plate reinforced opening at shear region with 15m span.
PB2-ROC-15			7.1	1618	135	Primary beam with CFRP reinforced opening at shear region with 15m span.
SB0-15	686×254×125	-	-	-	-	Reference secondary beam without opening or strengthening with 15m span.
SB1-UO-15		508.4×400.7	-	-	-	Secondary beam with unreinforced opening at mid-span with 15m span.
SB2-UO-15			-	-	-	Secondary beam with unreinforced opening at shear region with 15m span.
SB1-ROS-15			6	1010	80	Secondary beam with steel plate reinforced opening at mid-span with 15m span.
SB1-ROC-15			2.3	933	70	Secondary beam with CFRP reinforced opening at mid-span with 15m span.
SB2-ROS-15			6	1010	80	Secondary beam with steel plate reinforced opening at shear region with 15m span.
SB2-ROC-15			1.7	933	70	Secondary beam with CFRP reinforced opening at shear region with 15m span.

Key: PBn: primary beam, SBn: secondary beam, n = 0: no opening, n = 1: opening at mid-span, n = 2: opening near support, UO: unreinforced opening, ROC: CFRP reinforced opening, ROS: steel plate reinforced opening.

4.2 Modelling Approach

A similar modelling approach to that validating in Section 2 was used. S4R shell elements were employed to represent both the steel and CFRP, while element type COH3D8 was used for the adhesive material. Material properties for the CFRP and adhesive are given in Tables 1-3.

In order to simulate the support boundary conditions associated with a simple beam to column connection, a rigid plate was defined at the ends of the beam as shown in Figure 15. The plate was connected to the I-section through coupling constraints provided in ABAQUS using a reference point at the middle of the plate and mid-height of the I-section. The boundary conditions were then applied to the reference point [26]. For a simply supported condition, vertical and longitudinal restraints were applied at one end (to the reference point) while the other end was only restrained from vertical movement. This type of modelling can allow for any external axial load or bending moment to be applied at the support reference point without causing any eccentric loading condition. The beams were also laterally restrained along the top flange to prevent lateral torsional buckling. The adopted mesh used the same aspect ratio (i.e. number of elements per height of web and width of flange) as the optimum mesh from the validation study in Table 4.

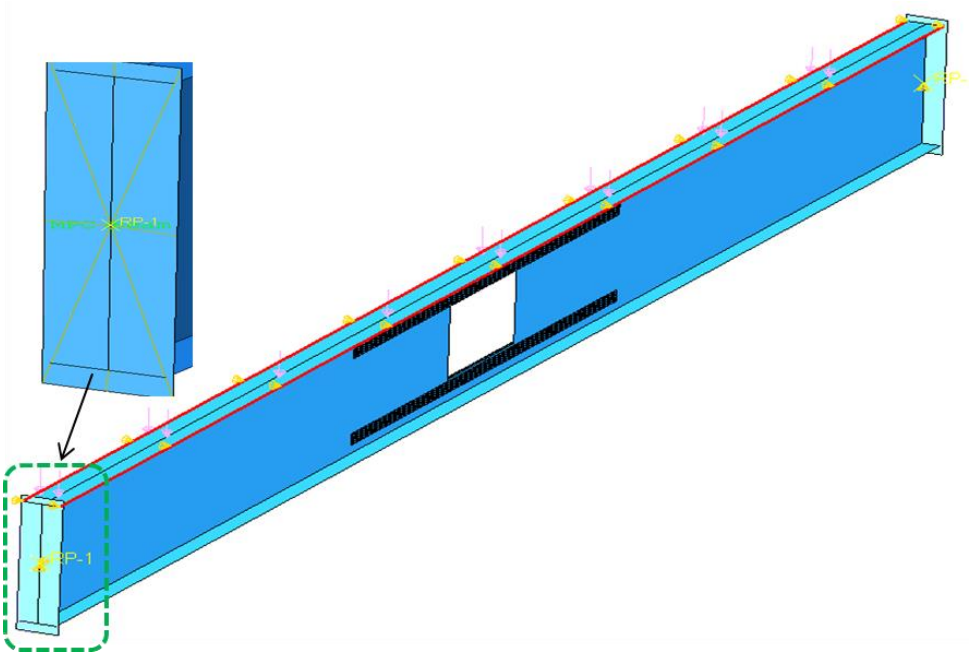

Figure 15: Use of rigid plate and coupling constraint for the support boundary conditions.

4.3 Simulation results

The results of the numerical study are now presented and discussed in terms of load-displacement behaviour, failure mode and behaviour of the strengthening system itself. All results have been compared with the control beams without openings and without strengthening in terms of applied load and failure mode.

4.3.1 Strength and Stiffness Effects

Firstly, as would be expected, the strength of both PBs and SBs for all floor arrangements dropped significantly after the introduction of a web opening at mid-span and for PBs at the maximum shear region, as summarised in Table 7. It can be seen from Tables 8 to 10 that strength was recovered completely after applying both types of strengthening, with a marginal increase occurring in some beams. However, the web opening at the shear region did not affect the strength of the secondary beams and no further strength was provided by using either type of strengthening. This reflects that the failure of these particular beams is dominated by flexure and the selected opening size in this area of the beam has minimal effect on the shear resistance of the SB2 series. All strengthened beams showed very similar stiffnesses to the corresponding un-strengthened reference beams. In all the CFRP strengthened cases, the ultimate load and load-displacement response is very similar (within +/- 5%) of the corresponding beams with steel stiffeners.

4.3.2 Modes of Failure

Since full lateral restraint was adopted for all the beams, no lateral torsional buckling (LTB) occurred. In addition, all beam cross-sections are either plastic or compact so all un-strengthened beams failed by a conventional flexural mode in which a plastic hinge forms at mid-span after top flange yielding, (Figure 16a,b and Figure 17a,b). For brevity the stress plots at ultimate load are shown in Figures 15 and 16 for the 7.5m series beams only, the other beam spans exhibited similar trends.

Regarding the un-strengthend beams with a web opening at mid-span, i.e. the PB1-U0 and SB1-U0 series, peak stresses occurred in the top T-section, this area was predominantly in compression and was therefore vulnerable to local buckling failure, see Figure 16c,d. In the corresponding CFRP strengthened beams, the CFRP was able to develop full composite action, reducing the local stresses at the T-section by around 30%. Similarly, the composite action allowed for redistribution of peak stresses to areas well away from the opening zone where plastic hinges eventually developed.

As previously mentioned, the introduction of a web opening in the shear region had no major effect on the strength and stiffness of the SB2-U0 series in which the failure mode was similar to the corresponding beam without an opening. In contrast, for the PB2-U0 series, a Vierendeel shear failure mode predominated whereby four plastic hinges developed around the corners of the opening, see Figure 17c,d. However, the corresponding CFRP strengthened beams, series PB2-ROC, exhibited typical flexural failure with a plastic hinge forming at the mid-span, Figure 17 h. As in the case of the B1-ROC series beams, full composite action between CFRP and steel allows for significant reduction in local stresses around the opening, and a shift in the plastic hinge well away from the opening zone.

4.3.3 Adhesive damage

Given the relatively high strengths of both steel and CFRP the most commonly observed failure mode of CFRP strengthened steelwork tends to be debonding [8] . With a view to

determining if the onset of debonding was likely in the series examined, the numerical stress degradation parameter, SDEG, was used to examine the damage status of the adhesive. Figures 18 and 19 show the SDEG parameter across the surface of the strengthening system for the 7.5m and 15m span beams respectively. In all cases the damage parameter is less than 1 (where 1 indicates debonding). Typically the highest values of the damage parameter occur at the edge of the plates and it is clear that some cases are close to deonding at ultimate load e.g. Figure 18b. These results indicate the chosen CFRP thickness and bond length are effectively proportioned so as to ensure full composite action up to ultimate load.

4.3.4 CFRP strain distribution

Figures 20 and 21 show the strain distribution in the CFRP system at ultimate load for the 7.5m and 15m span beams. In the case of the beams with mid-span openings, the highest strains are recorded in the region immediately around the opening itself (Figures 20 and 21 a and b). For the CFRP attached to the top and bottom flanges in the B1-ROC series, the strain distribution is relatively even. The strains in all cases are well below rupture. For the B2-series beams, concentration of high strains are observed in the web mounted plates close to the opening corners, reflecting the Vierendeel action. Some of the strain concentrations in the aforementioned locations are approaching the ultimate strain in the case of the 15m span, Figure 21(d).

The utilisation ratio can be used as a basic measure of the efficiency of the plate, the ratio is defined as the CFRP strain/CFRP rupture strain. The CFRP utilisation ratio ranged from 20-70% and 24-85% for the 7.5m beams and 15m beams respectively, ratios for specific beams are presented in Table 11. It is clear from Table 11 that for the majority of the beams with central web openings, the CFRP is comparatively lowly stressed, this suggests reductions in plate thickness or use of a lesser grade FRP made be appropriate here. The highest strain concentrations occur in the primary beams with web openings near the end supports, the very localised nature of these suggest a local thickening of the strengthening plate may be the most efficient strengthening solution.

4.3.5 Steel stiffeners' stress distribution

To gain an understanding of how the steel stiffeners are working, the Von Mises stress at ultimate load is presented in Figures 22 and 23 for the 7.5 and 15m spans respectively. In the case of the B1-ROS series, a relatively uniform distribution of stress is observed across the flange mounted stiffeners. While in the case of the B2-ROS series, stresses localised around the corners of the opening can be seen. In all cases, yielding of the stiffeners did not occur.

5. Conclusions

After validation of the modelling technique against experimental data, several numerical simulations have been conducted in this work to explore the ability of CFRP strengthening to recover the stiffness and strength of full-scale steel floor beams after the introduction of a web opening. In addition, the performance of CFRP

strengthening has been compared with conventional steel-plate strengthening. Three spans commensurate with a typical commercial steel frame building were considered i.e. 7.5m, 10m and 15m. Additionally two different web opening locations, one in an area of high shear and the other in an area of higher bending, were investigated. The findings of this study can be summed up as follows:

1. For the beam configurations examined, the CFRP-strengthening method is able to recover stiffness and strength after insertion of a web opening to that of the beam without web openings. This applies whether the opening is at mid-span or at the beam ends in the regions of high shear. This finding suggests CFRP is a suitable, practical and economic way of strengthening beams are in-service changes that result in web openings being added.

2. Full composite action between the steel section and CFRP was achieved in all the strengthened beams examined. This resulted in reduction of high stresses around the web openings and allowed the development of plastic hinges well away from the opening zone. This points to the need to check capacity not just in the region of strengthening for expected failure modes (e.g. Vierendeel action) but also at other locations and for other failure modes (e.g. plastic bending). This finding for the cases studied numerically is in line with earlier findings from the smaller-scale experimental work [17].

3. In all CFRP strengthened cases debonding did not occur. Typically, debonding occurs where there is insufficient bond length for the plate to be effectively mobilised. The concentration of high shear stresses at the plate ends is also a key factor in onset of debonding. The absence of debonding points towards adequacy of the adopted plate length and thickness in the configurations examined.

4. The CFRP configurations examined were able to match the performance of the corresponding traditional steel plate strengthened beams in terms of ultimate load, stiffness and failure modes. This suggests that the use of CFRP in practical quantities can compete with steel plates when applied to web openings in floor beams of a scale typically used in modern frame structures. Clearly the potential is there, however more extensive investigation is required to develop adequate design guidance, particularly with a view to optimisation of plate thickness and length given the relative expense of CFRP material compared to steel. While the relative material cost of the proposed CFRP arrangements may exceed that of the steel strengthening examined in this study, the ease of application of a surface bonded CFRP plate in the case of existing steel floor beams (as opposed to in-situ welding of steel plate stiffeners) and the whole life performance of the material are likely to produce savings.

Aknowledgements:

The authors wish to thank the Iraqi Ministry of Higher Education and the University of Babylon in funding this research. Similarly the contribution of the School of Mechanical, Aerospace and Civil Engineering at the University of Manchester is gratefully acknowledged.

Table 7 Percentages of strength reduction due to web opening.

PB1-UO-7.5	12%	PB2-UO-7.5	25%	SB1-UO-7.5	14%	SB2-UO-7.5	0%
PB1-UO-10	20%	PB2-UO-10	37%	SB1-UO-10	22%	SB2-UO-10	0%
PB1-UO-15	24%	PB2-UO-15	19%	SB1-UO-15	13%	SB2-UO-15	0%

Table 8: Load versus mid-span deflection of 7.5m floor beams.

	PB	SB
Opening at midspan	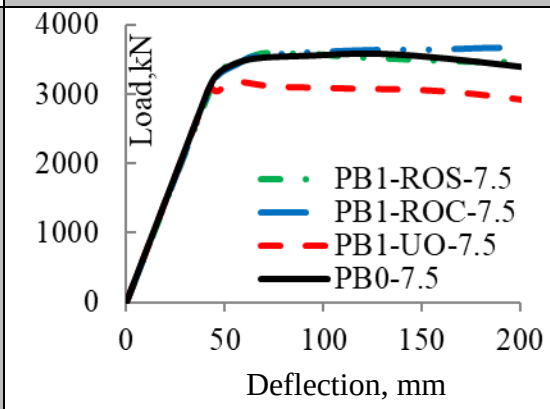	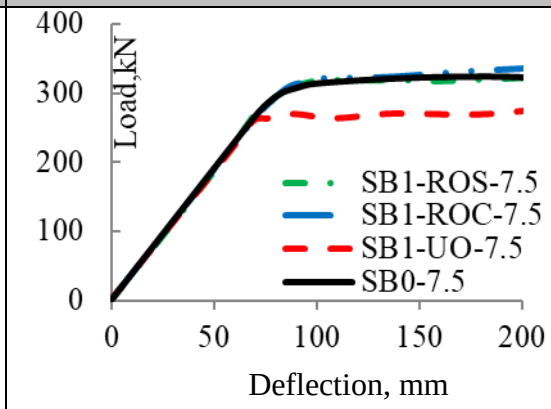
Opening at shear side	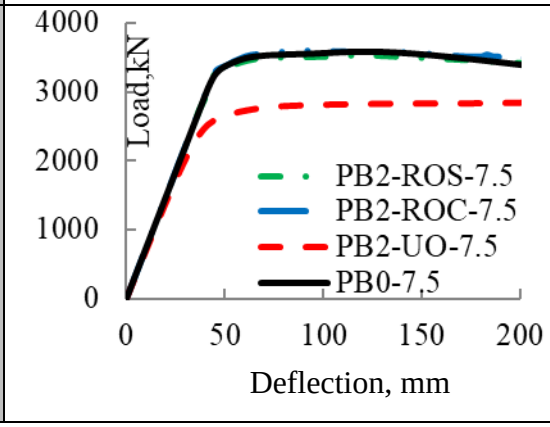	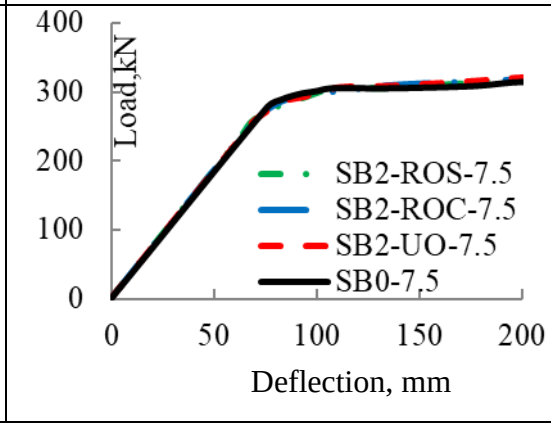

Table 9: Load versus mid-span deflection of 10m floor beams.

	PB	SB
Opening at midspan	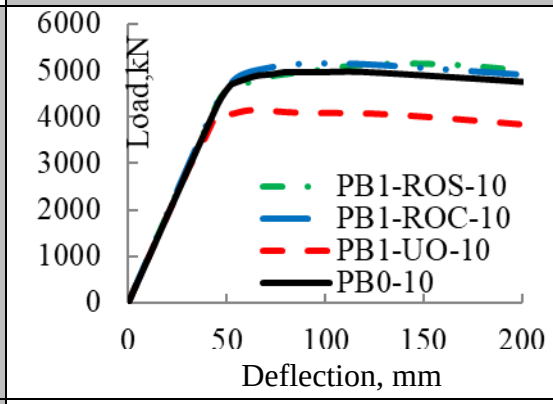	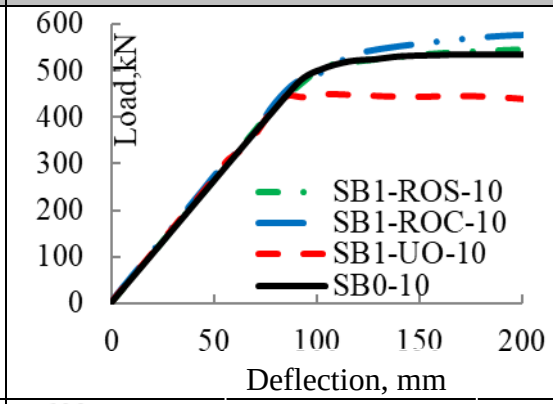
Opening at shear side	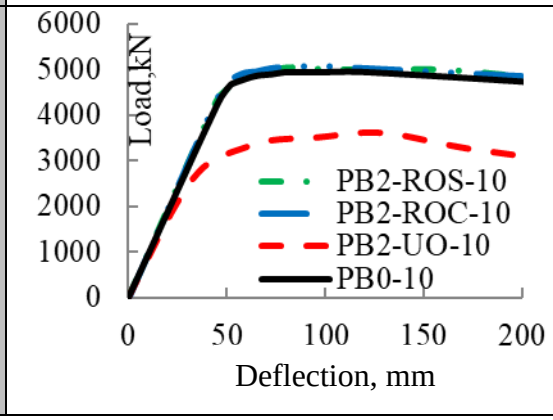	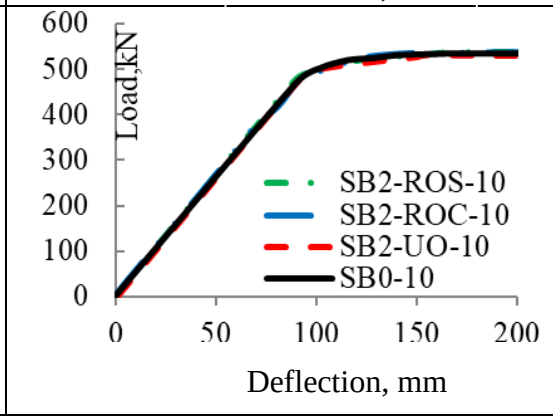

Table 10: Load versus mid-span deflection of 15m floor beams.

	PB	SB
Opening at midspan	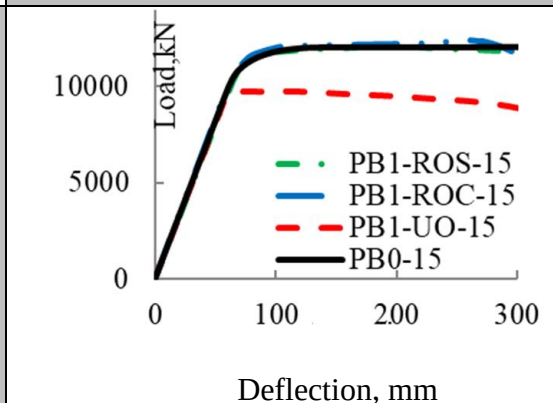	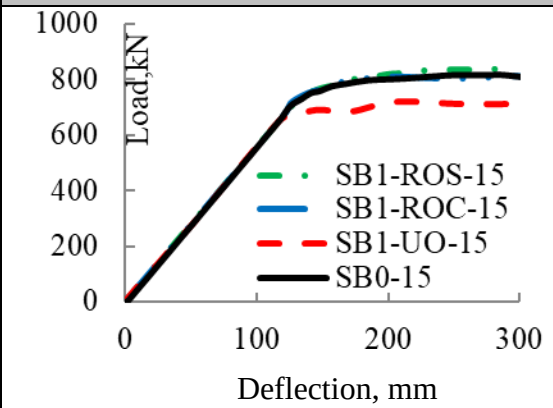
Opening at shear side	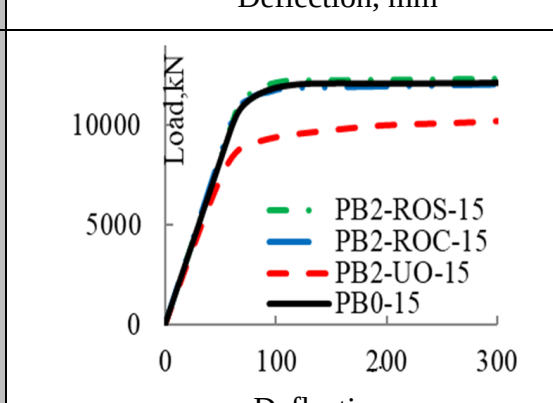	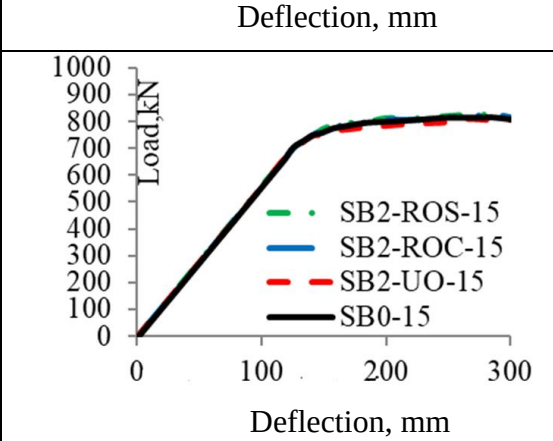

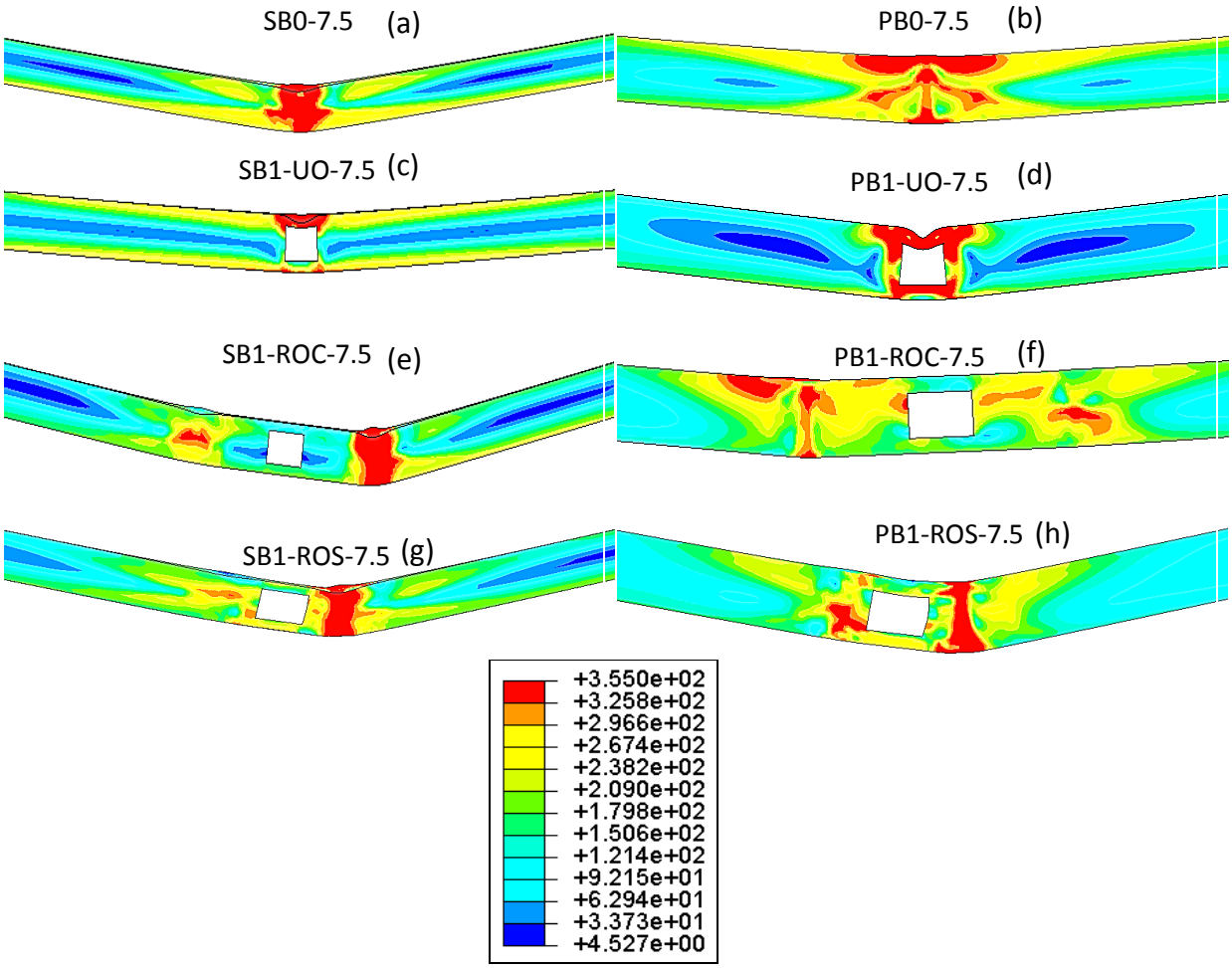

Figure 16: Deflected shape and von-Mises stresses (MPa) at maximum load for 7.5m beams with web opening at mid-span.

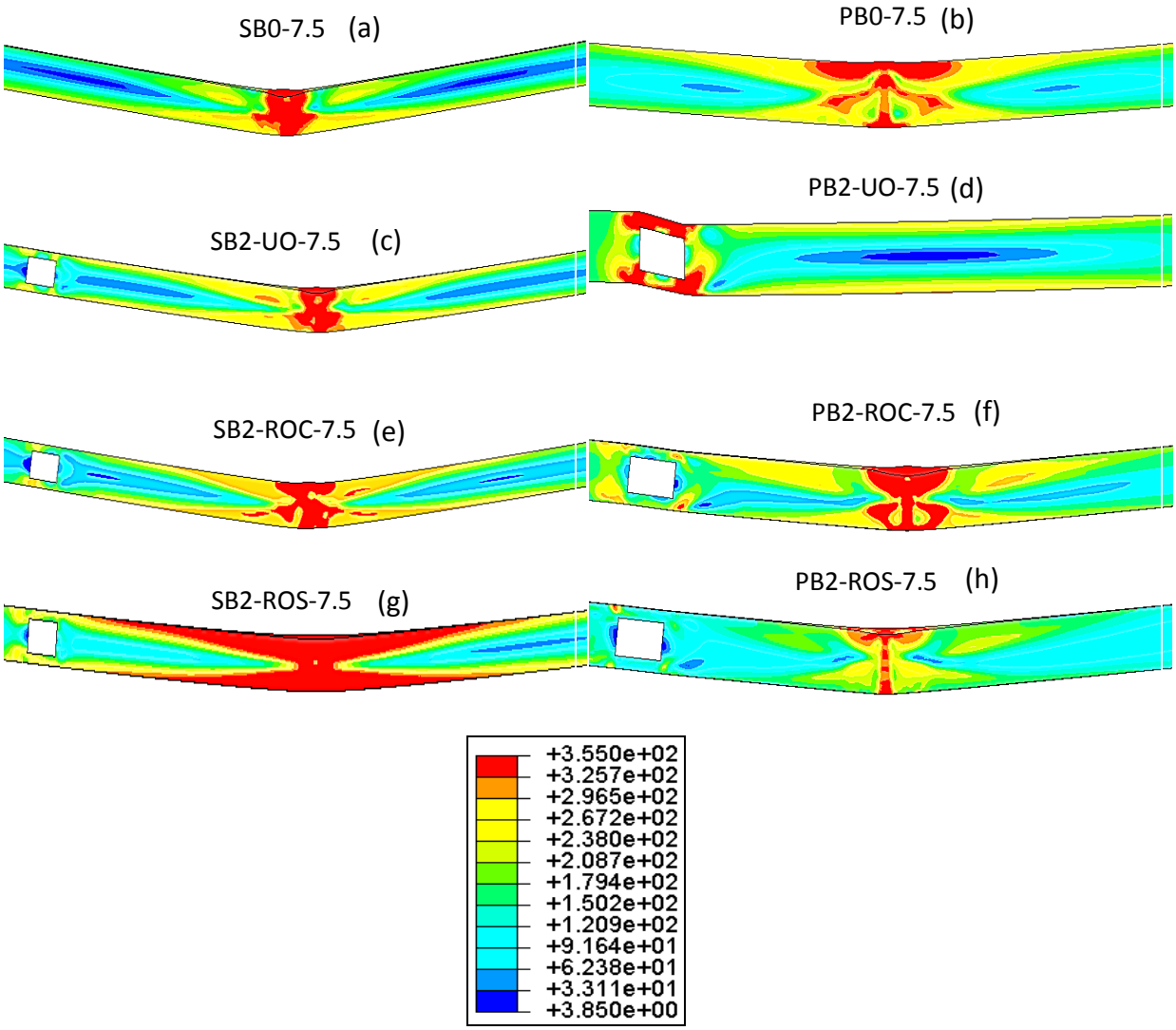

Figure 17: Deflected shape and von-Mises stresses (MPa) at maximum load for 7.5m beams with web opening near support.

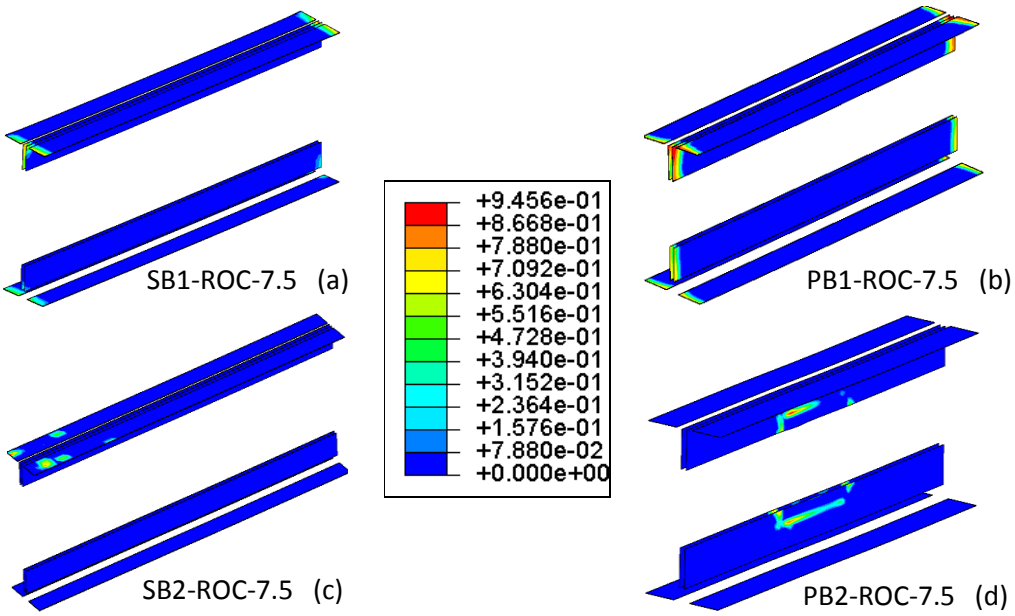

Figure 18: Adhesive damage parameter, SDEG, for 7.5m beams at maximum load (note a value of 1 indicates debonding).

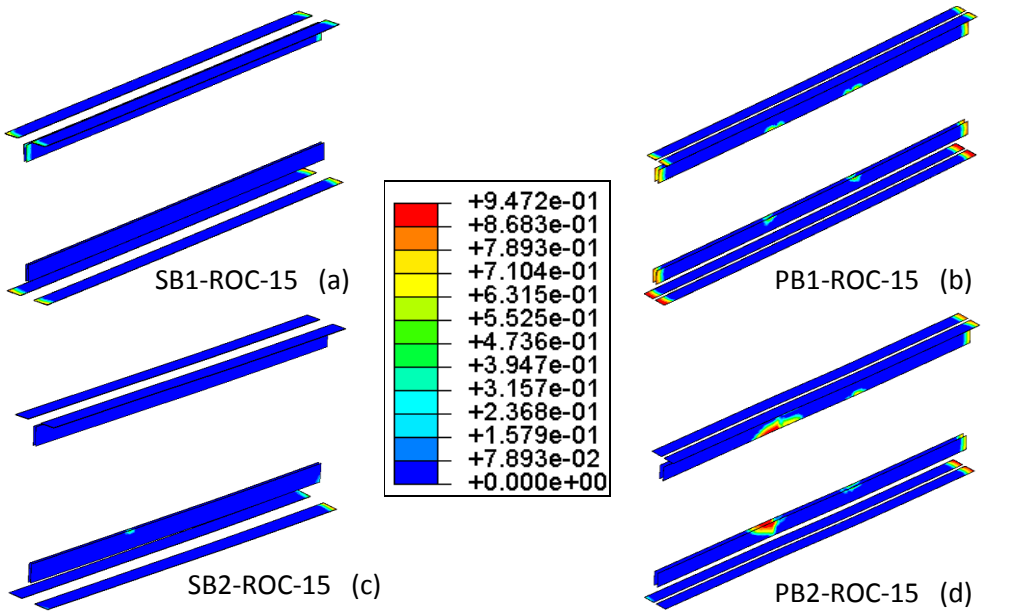

Figure 19: Adhesive damage parameter, SDEG, for 15m beams at maximum load.

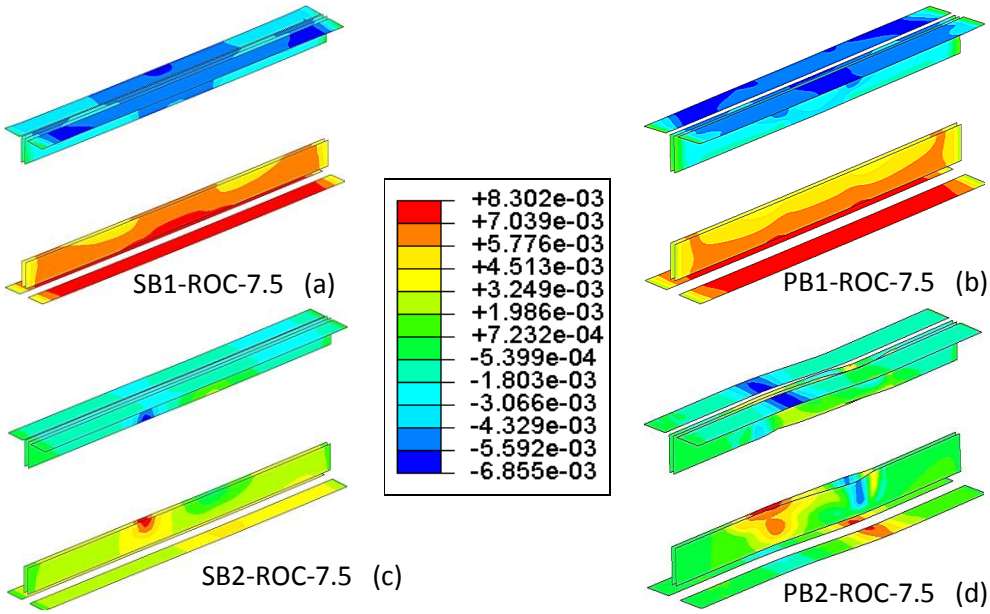

Figure 20: Strain distribution on CFRP plates at maximum load for 7.5m beams

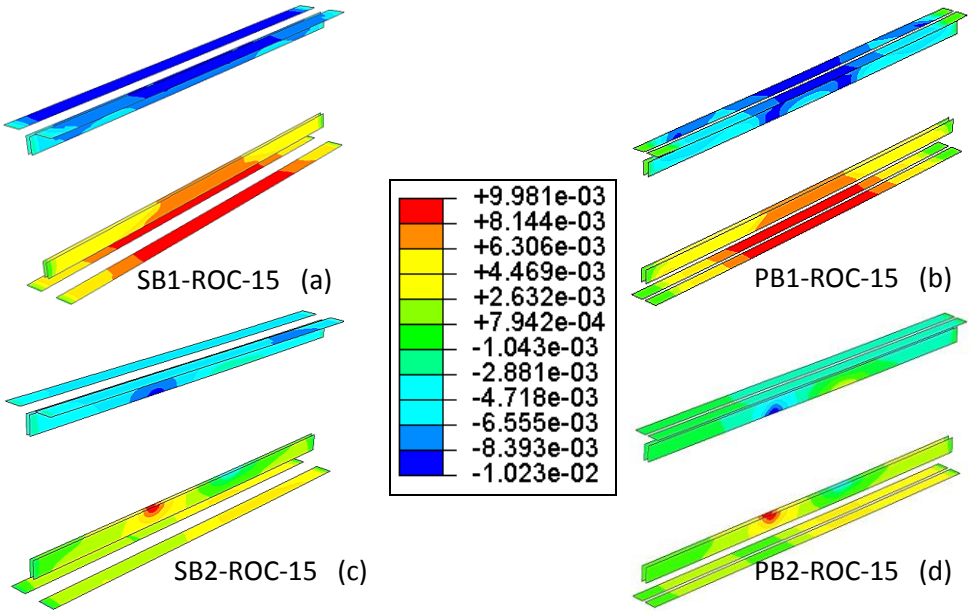

Figure 21: Strain distribution on CFRP plates at maximum load for 15m beams.

Table 11 Utilisation percentages of CFRP in different beams.

7.5m				10m				15m			
Mid-span opening		Shear side opening		Mid-span opening		Shear side opening		Mid-span opening		Shear side opening	
SB	PB	SB	PB	SB	PB	SB	PB	SB	PB	SB	PB
20	24	31	70	22	26	34	75	24	29	41	85

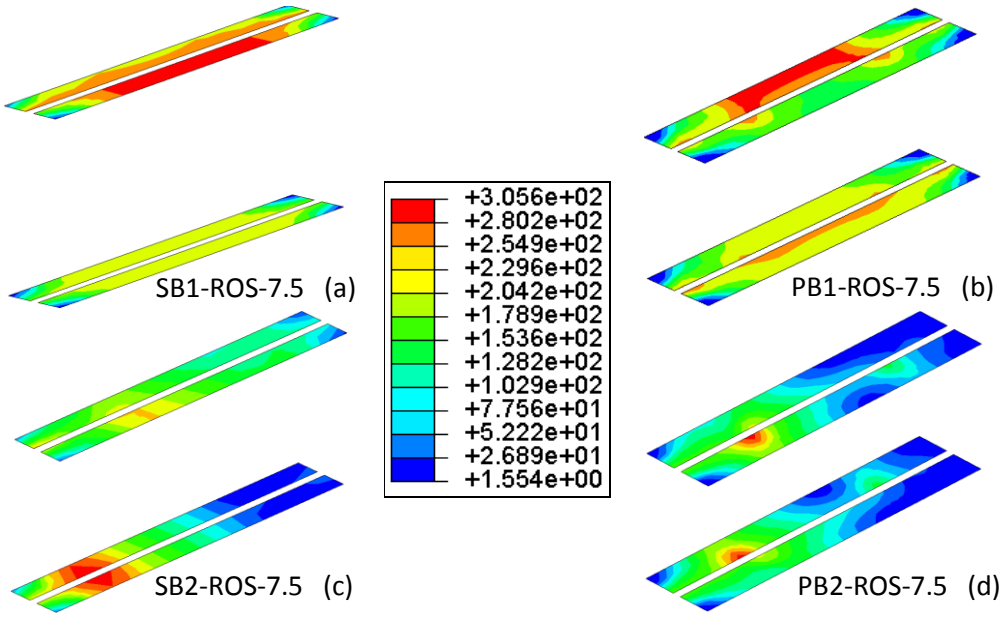

Figure 22: Von Mises stress distribution (N/mm^2) on steel stiffeners at maximum load for 7.5m beams.

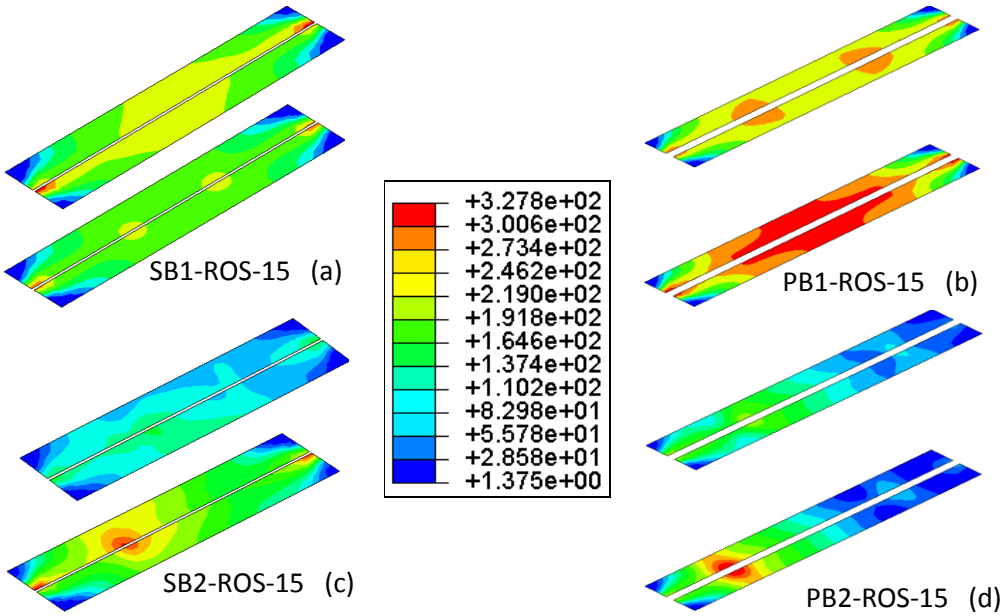

Figure 23: Von Mises stress distribution (N/mm^2) on steel stiffeners at maximum load for 15m beams.

Table 12 Utilisation percentages of steel plates in different beams.

7.5m				10m				15m			
Mid-span opening		Shear side opening		Mid-span opening		Shear side opening		Mid-span opening		Shear side opening	
SB	PB	SB	PB	SB	PB	SB	PB	SB	PB	SB	PB
70	79	77	86	62	94	60	88	83	90	78	92

References

1. A. Shaat , D. Schnerch, A. Fam, S. Rizkalla, Retrofit of steel structures using Fiber-Reinforced Polymers (FRP): State-of-the-art. In: Transportation research board (TRB) annual meeting, 2004.
2. W. Edberg, D. Mertz, J. Gillespie, Rehabilitation of Steel Beams Using Composite Materials. Proceedings of the Materials Engineering Conference, Materials for the New Millenium, ASCE, New York, NY, Nov 10-14, pp. 502 508, 1996.
3. J. Deng, M.M.K. Lee, Behaviour under static loading of metallic beams reinforced with a bonded CFRP plate, Compos. Struct. 78 (2), pp.232–242, 2007.
4. J. Gillespie, D. Mertz, K. Kasai, W. Edberg, J. Demitz, I. Hodgson, Rehabilitation of Steel Bridge Girders: Large Scale Testing. Proceeding of the American Society for Composites 11th Technical Conference on Composite Materials, pp. 231-240, 1996.
5. M. Tavakkolizadeh, H. Saadatmanesh, Repair of cracked steel girders using CFRPsheets, ISEC-01, Hawaii, 2001.
6. M. Bocciarelli, Fatigue performance of tensile steel members strengthened with CFRP plates. Composite Structures, 87(4), pp.334–343, 2009.
7. M. Youssef, Analytical prediction of the linear and nonlinear behaviour of steel beams rehabilitated using FRP sheets. Engineering structures, 28(6), pp.903–911, 2006.
8. X. Zhao, L. Zhang, State-of-the-art review on FRP strengthened steel structures. Engineering Structures, 29, pp.1808–1823, 2007.
9. He J, Xian G. Debonding of CFRP-to-steel joints with CFRP delamination. Composite Structures, 153, pp.12-20, 2016.
10. F. Kianmofrad, E. Ghafoori, M.M. Elyasi, M. Motavalli & M. Rahimian, Strengthening of metallic beams with different type of pre-stressed un-bonded retrofit systems, Composite Structures, 159, pp. 81-95, 2017.
11. E. Gafoori, M. Motavalli, A. Nussbaumer, A. Herwig, G.S. Prinz & M. Fontana, Design criterion for fatigue strengthening of riveted beams in a 120-year-old railway metallic bridge using pre-stressed CFRP plates, Composites Part B, 68, 2015, pp. 1-13.
12. A. Hosseini, E. Ghafoori, M. Motavalli, A. Nussbaumer, X. Zhao & R. Al-Mhaidi, Flat pre-stressed unbonded retrofit system for strengthening of existing metaillic I-Girders, Composites Part B, 155, pp. 156-172, 2018.
13. A. M. Mahmoud, Full bonded shear and flexural CFRP strengthening of steel I-beams with and without openings, Journal of Engineering and Applied Science, 59 (6), Cairo University, pp. 493-515, 2012.
14. M. Hamood, W. AbdulSahib and A. Abdullah, The effectiveness of CFRP strengthening of steel plate girders with web opening subjected to shear, MATEC Web Conf., 162, 04012, 2018.

15. M. Altaee, L. Cunningham, M. Gillie, Novel technique for strengthening steel beams with web penetrations, Proceedings of the MACE PGR Conference, University of Manchester, UK, pp. 9–11, 2016.
16. M. Altaee, L. Cunningham, M. Gillie, CFRP strengthening of steel beams with web openings, Proceedings of Structural Faults & Repair 2016: 16th International Conference, Edinburgh, UK, p.1754, 2016.
17. M. Altaee, L. Cunningham, M. Gillie, Experimental investigation of CFRP-strengthened steel beams with web openings, Journal of Constructional Steel Research. 138, pp.750-760, 2017.
18. F. Bowden, D. Tabor, The friction and lubrication of solids, Oxford university press, 2001.
19. A. Al-Mosawe, R. Al-Mahaidi & X Zhao, Bond behaviour of CFRP laminates and steel members under different loading rates, Composite Structures, 148, pp. 236-251, 2016.
20. Huntsman, Araldite 420A/B, Product data, Huntsman International LLC, 2009.
21. M.M.A. Kadhim, Z. Wu & L.S. Cunningham, Experimental and numerical investigation of CFRP strengthened steel beams under impact load, ASCE Journal of Structural Engineering, in-press, 2019.
22. ABAQUS, Theory Manual, User Manual and Example Manual, Version 6, Dassault Systems Simulia Corp., 2013.
23. BS EN 1993-1-1, Eurocode 3: Design of Steel Structures, British Standards Institution, London, UK, 2005.
24. BS EN 1991-1-1, Eurocode 1: Actions on structures - Part 1-1: General actions, Densities, self-weight, imposed loads for buildings, British Standards Institution, London, UK, 2009.
25. Lawson, R.M. & Hicks, S.J., Design of beams with large web openings, SCI P355, The Steel Construction Institute, UK., 2011
26. M. Najafi, Y. Wang, Axially restrained steel beams with web openings at elevated temperatures, part 2: Development of an analytical method. Journal of Constructional Steel Research, 128, pp.687–705, 2017.